189664

61

N94-14749

Search for subgrid scale parameterization by projection pursuit regression

By C. Meneveau[1], T. S. Lund[2] AND P. Moin[2]

The dependence of subgrid-scale stresses on variables of the resolved field is studied using direct numerical simulations of isotropic turbulence, homogeneous shear flow, and channel flow. The projection pursuit algorithm, a promising new regression tool for high-dimensional data, is used to systematically search through a large collection of resolved variables, such as components of the strain rate, vorticity, velocity gradients at neighboring grid points, etc. For the case of isotropic turbulence, the search algorithm recovers the linear dependence on the rate of strain (which is necessary to transfer energy to subgrid scales) but is unable to determine any other more complex relationship. For shear flows, however, new systematic relations beyond eddy viscosity are found. For the homogeneous shear flow, the results suggest that products of the mean rotation rate tensor with both the fluctuating strain rate and fluctuating rotation rate tensors are important quantities in parameterizing the subgrid-scale stresses. A model incorporating these terms is proposed. When evaluated with direct numerical simulation data, this model significantly increases the correlation between the modeled and exact stresses, as compared with the Smagorinsky model. In the case of channel flow, the stresses are found to correlate with products of the fluctuating strain and rotation rate tensors. The mean rates of rotation or strain do not appear to be important in this case, and the model determined for homogeneous shear flow does not perform well when tested with channel flow data. Many questions remain about the physical mechanisms underlying these findings, about possible Reynolds number dependence, and, given the low level of correlations, about their impact on modeling. Nevertheless, demonstration of the existence of causal relations between sgs stresses and large-scale characteristics of turbulent shear flows, in addition to those necessary for energy transfer, provides important insight into the relation between scales in turbulent flows.

1. Introduction

Of central importance to the numerical simulation of the large scales in turbulent flows is the proper parameterization of the subgrid-scale (sgs) stress deviator, defined as

$$\tau_{ij} \equiv \widetilde{u_i u_j} - \tilde{u}_i \tilde{u}_j - \frac{1}{3}(\widetilde{u_k u_k} - \tilde{u}_k \tilde{u}_k)\delta_{ij}, \qquad (1)$$

1 Johns Hopkins University
2 Center for Turbulence Research

as a function of the resolved velocity field $\tilde{u}_i$. Here $\tilde{()}$ represents spatial filtering at a particular scale r. The most widely used model is Smagorinsky's (1963):

$$\tau_{ij} = -2 \, C_s^2 \, r^2 \, \sqrt{2\tilde{S}_{ij}\tilde{S}_{ij}}, \tag{2}$$

where

$$\tilde{S}_{ij} = \frac{1}{2} \left(\frac{\partial \tilde{u}_i}{\partial x_j} + \frac{\partial \tilde{u}_j}{\partial x_i} \right) \tag{3}$$

is the strain rate of the resolved motion. The model constant C_s can be prescribed or can be determined dynamically based on information provided by the resolved field, as in the recently developed dynamic model (Germano *et al.*, 1991).

Although the Smagorinsky model has been in use for nearly thirty years, for roughly half that period it has been known that the model provides only a very crude estimate for the stresses. This fact was first demonstrated by Clark *et al.* (1979), where direct numerical simulation (DNS) data for homogeneous isotropic turbulence was used to evaluate model predictions. Clark *et al.* found a correlation coefficient of approximately 0.2 when comparing predictions of the Smagorinsky model with the exact stresses. McMillan *et al* (1979) found that the correlation coefficient was even lower in homogeneous shear flow, being of order 0.1. Later, Piomelli *et al.* (1988) found similar results in turbulent channel flow.

When contemplating these extremely low correlation coefficients, it may seem striking that the Smagorinsky model works at all. Of course, the resolution of this paradox is that, by construction, the Smagorinsky model insures that there will be a net drain of energy from the large scales to the subgrid-scale motions. This is the primary objective of a subgrid-scale model, and as long as this requirement is met, reasonable results may be expected. On the other hand, the Smagorinsky model provides poor predictions of the individual elements of the stress tensor. It is natural to expect that superior results could be obtained with a model that yields a more accurate prediction of the stress tensor. The objective of this work is to seek out potentially more accurate models.

The Smagorinsky model relates the subgrid-scale stress with only the resolved strain rate. It is reasonable to expect that the stresses might also depend on other resolved quantities such as the vorticity. If simple models based on a limited number of such quantities are postulated, conventional least-squares fitting techniques can be used to test the modeling hypothesis. Such a test was performed by Lund and Novikov (1992), where the stresses were assumed to depend on the anti-symmetric as well as the symmetric part of the velocity gradient tensor (rotation rate and strain rate tensors, respectively). It was shown that the stress tensor could be expanded in a series formed from products of these two tensors. Tests of this expansion in isotropic turbulence revealed that inclusion of rotation rate did not significantly improve the model prediction. The results of Lund and Novikov thus suggest that it is necessary to search for other quantities on which the stresses could depend. Velocity gradients taken at neighboring points or perhaps gradients filtered at different (larger) scales are possible candidates which would not violate Galilean invariance.

Unfortunately, as the list of possible independent variables increases, the task of finding statistically meaningful relations from the DNS data becomes unmanageable. In principal, if a multidimensional scatter-plot of τ_{ij} as a function of several independent variables is generated, a high-dimensional cloud of points would be obtained. This may (or may not) exhibit some clustering around a most probable behavior. If such a hypersurface exists about which the data appears preferentially clustered, it would constitute a clear basis for modeling. However, finding such a surface from the DNS data represents a difficult problem of regression in a high-dimensional space of variables. Parametric regression, such as least-square error fitting to some assumed functional form, is quite difficult because there is little indication as to what such a function should be. Finding the surface by dividing the high-dimensional space into small hypercubes and performing local smoothing of the data is impractical because even large amounts of data become extremely sparse in a high-dimensional setting (curse of dimensionality).

Although the challenges in performing a high-dimensional regression are apparent, recent advances in statistical science allow such problems to be tackled. An elegant method that circumvents many problems inherent to high-dimensional regression was proposed by Friedman & Stuetzle in 1981. Known as the Projection Pursuit Regression algorithm, this method was originally developed to analyze experimental data in particle physics involving a large number of variables. The algorithm consists of a numerical optimization routine that finds one dimensional projections of the original independent variables for which the best correlations with the dependent variable can be obtained. The dependent variable can then be written as a sum of empirically determined functions of the projections. We shall use the projection pursuit regression algorithm to investigate relationships between the subgrid-scale stresses and quantities in the resolved field.

In section 2, we briefly summarize the projection pursuit method, present an illustrative example, and comment on both its strengths and weaknesses. Section 3 describes applications to isotropic turbulence, both decaying and forced. Section 4 presents applications to homogeneous turbulent shear flow and section 5 to channel flow simulations. The results obtained from these anisotropic flows suggest possible modeling strategies that are explored at the end of sections 4 and 5. Section 6 summarizes this work and presents the conclusions.

2. Review of projection pursuit regression

The problem is to find the 'best' relation between a 'response' y and a set of predictor variables x_1, x_2,...x_n. In our problem, y will be identified with each of the elements of the sgs stress tensor, and the x_i's will be the elements of resolved rate of strain, vorticity, etc., i.e. all the variables that the stresses are assumed to depend upon. When performing tests with DNS data, there will be a large number of realizations (essentially at every grid-point) of the 'response variable' τ (y) and of the 'predictor variables' strain rate, vorticity, etc (x_i, $i = 1, 2...n$).

Friedman & Stuetzle (1981) summarize the inherent problems of traditional methods, such as parametric regression and regression based on local smoothing. With

the former, one has to assume a particular functional form and determine unknown coefficients or parameters by some method such as least-square error fitting. Since we do not wish to impose such relationships *a priori*, this is not a method of choice. Local smoothing consists of fitting a hypersurface in a small hypercube of data and repeating this in each cube. The regression surface is then the union of all these local fits. In high-dimensional settings, this is practically impossible. Consider the following example (Friedman & Stuetzle, 1981). Let $\mathbf{x} \in \mathbf{R}^{10}$, i.e. $n = 10$. If the width of the cube used for the local smoothing spans 10% of the range of each variable, each cube will contain typically only a fraction equal to 0.1^{10} of the data, which is too sparse. On the other hand, if one requires each hypercube to contain 10 % of the data, then the window has to span $0.1^{0.1} \sim 80\%$ of the range of the predictor variables, which is too large.

Projection pursuit regression (ppreg henceforth) circumvents these difficulties by projecting the high-dimensional data onto a single variable $z = \alpha_1 x_1 + \alpha_2 x_2 + ... + \alpha_n x_n$. Local smoothing is then performed to obtain an empirically determined function $f(z)$ that follows the main trend of the data as a function of z. The smoothing algorithm is described in Friedman & Stuetzle (1981) and consists of several passes over the data (y as a function of z) to adjust the bandwidth of the smoothing to the local conditions. The variance $\sigma_\alpha^2 =< (y - f(z))^2 > - < (y - f(z)) >^2$ of the data around $f(z)$ is computed. The core of the algorithm is a numerical optimization procedure in which the coefficients α_i are selected so as to *minimize* the variance σ_α^2. Let the α's thus found be denoted by $\alpha_i^{(1)}$, and let $z^{(1)}$ and $f^{(1)}(z^{(1)})$ be the corresponding univariate projection and the empirical function giving a good fit for y as a function of $z^{(1)}$. The procedure is repeated for the residues, defined as $y - f^{(1)}(z^{(1)})$, and a new projection $\alpha_i^{(2)}$ and a smooth empirical function $f^{(2)}(z^{(2)})$ are found. This procedure is repeated until the variance stops to decrease appreciably by adding new projections. Finally, the model consists of the sum

$$y_{mod} = \sum_{m=1}^{M} f^{(m)}(\alpha_1^{(m)} x_1 + \alpha_2^{(m)} x_2 + .. + \alpha_n^{(m)} x_n). \tag{4}$$

For the case that the response variable is a linear combination of x_i (i.e. $y = \beta_1 x_1 + ... \beta_n x_n$), ppreg reduces to the usual n-dimensional linear least-square error fit (where the α's are the coefficients and $f^{(1)}$ is a linear function). In general however, the functions $f^{(m)}$ need not be linear. The fundamental advantage of this procedure is illustrated in the following example. If y is the product of x's, say $y = x_1 x_2$, then this can be represented as a sum of two univariate functions according to $y = \frac{1}{4}(z^{(1)})^2 - \frac{1}{4}(z^{(2)})^2$, where $z^{(1)} = x_1 + x_2$ and $z^{(1)} = x_1 - x_2$. The ppreg algorithm is thus able to find some nonlinear relations without stipulating them *a priori*.

As an illustrative example, we consider 1000 realizations of a ten-dimensional random vector $\mathbf{x}$ where each x_i is normally distributed with zero mean and unit variance. Then y is prescribed as follows:

$$y = x_3 x_4 + \tanh(x_6 + x_7) + \xi, \tag{5}$$

where ξ is another Gaussian random variable with zero mean and variance of 0.1. However, ξ is not included in the list of predictor variables x_i and, therefore, represents extraneous noise. Projection pursuit is applied to this artificially generated set of data. The projections found by ppreg are, successively: $\alpha_6^{(1)} = 0.69$, $\alpha_7^{(1)} = 0.72$; $\alpha_3^{(2)} = 0.66$, $\alpha_4^{(2)} = 0.74$; and $\alpha_3^{(3)} = -0.67$, $\alpha_4^{(3)} = -0.73$; other α's are negligible. The empirical functions (solid lines) resemble the tanh function in the first projection, parabolas in the latter two. The projected data are shown in Figures 1(a) to (c). If we least-square error fit a *tanh* profile through Figure 1(a), we obtain $y_1 = 1.1 tanh[1.3(0.69x_6 + 0.72x_7)]$. The scatter plot in Figure 1(b) is then $y - y_1$ *vs* the second projection $z^{(2)} = 0.66x_3 + 0.74x_4$. Parabolic fits through Figures 1(b) and 1(c) give $y_2 = 0.4(0.66x_3 + 0.74x_4)^2$ and $y_3 = -0.4(-0.67x_3 + 0.73x_4)^2$. (These fits are not exactly equal to the empirical smoothing functions constructed by the algorithm, this being the reason why the scatter plot of Figure 1(c) falls below the smooth.) The final model then consists of $y_1 + y_2 + y_3$ which is plotted with the original y in Figure 1(d).

The residual noise is mainly due to the non-deterministic dependence of y with respect to ξ. The initial correlation coefficient between y and e.g. x_4 was 0.012, while the correlation coefficient between y and the model, y_{mod}, is now $\rho = 0.96$. Finding such a non-trivial dependence from few data points in a 10-dimensional space is quite remarkable.

Although impressive in the above example, ppreg is not fool-proof. For cases when y depends on the x_i's in ways that cannot be written as sums of functions of linear combinations of x_i's (such as divisions), ppreg is usually unable to find good projections. Therefore, while the method works remarkably well for an entire family of non-trivial relations, it cannot be considered entirely general.

In addition to application to sgs modeling to be reported in the following pages, we believe that the ppreg method should be applicable to a host of other problems where large amounts of data need to be analyzed and functional dependencies established (Reynolds-stress modeling, reacting flows, control, etc.).

3. Isotropic turbulence

In this section, ppreg is used to search for possible functional dependence between the residual stresses and a host of resolved variables in homogeneous isotropic turbulence. Both decaying and forced isotropic turbulent fields are considered.

3.1 Flow-fields and calculations

Both the forced and decaying isotropic turbulent fields were generated on a 128^3 mesh with the pseudo-spectral code of Rogallo (1981). For the decaying turbulence, the energy spectrum was initialized according to

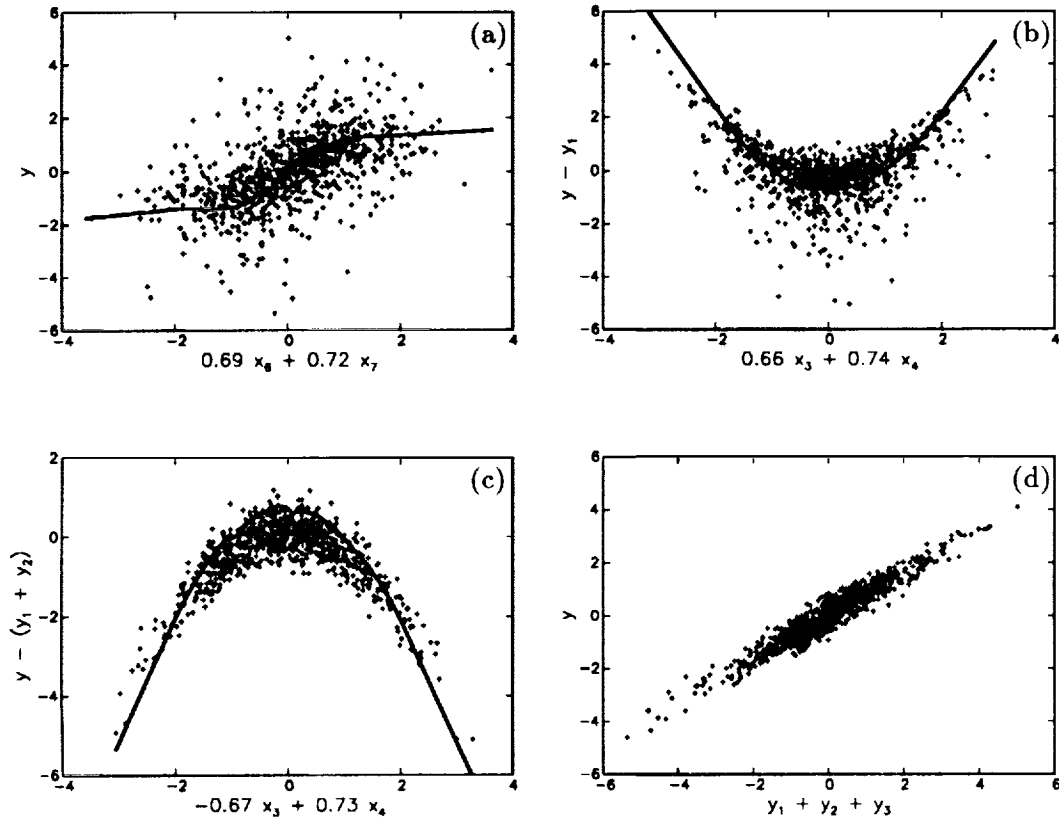$$E(k) = \frac{1}{32} \left(\frac{k}{2}\right)^4 \exp\left(-\frac{k}{2}\right).$$

FIGURE 1. Illustrative application of ppreg to a test case. (a) Response y as a function of first projection $z^{(1)} = 0.69x_6 + 0.72x_7$ (symbols) and mean trend $f^{(1)}(z^{(1)})$ found by local smoothing (solid line). (b) Second projection of $y - y_1$, where y_1 has been found by fitting a *tanh* profile through Figure 1(a). Solid line: $f^{(2)}(z^{(2)})$ found by the algorithm. (c) Third projection and $f^{(3)}(z^{(3)})$. (d) Response variable y as a function of the sum of empirically determined fits in (a), (b) and (c).

This spectrum has its energy peak at wavenumber 8. The initial phases for the complex velocity field were chosen randomly but in such a way that the divergence-free condition was satisfied (see Rogallo, 1981 for more details on the initial conditions).

In order to develop realistic turbulence from the random phase initial condition, the flow was allowed to evolve freely for 2.9 small scale eddy turnover times, τ_{t_0} (based on quantities derived from the end of the initial run; $\tau_{t_0} = \frac{\lambda_0}{u'_0}$ where λ_0 and u'_0 are the Taylor microscale and the rms turbulence intensity, respectively). Over this period of time, the total turbulent kinetic energy decayed by 34%. The Taylor microscale Reynolds number $(u'\lambda/\nu)$ was 45.3, and the velocity derivative skewness was −0.32. The 3-D radial energy spectrum at the end of the run is plotted in
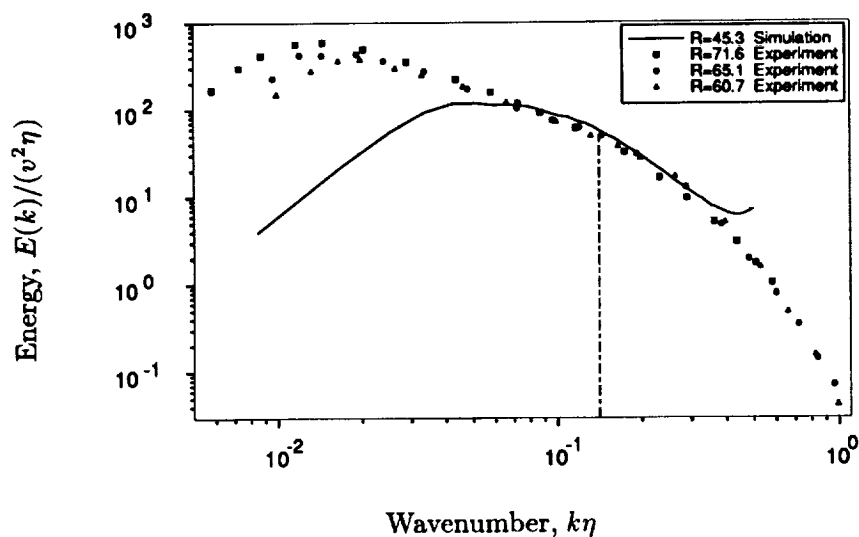
FIGURE 2.   3-D radial energy spectrum for the decaying isotropic turbulence, plotted in Kolmogorov units. The experimental data were taken from Comte-Bellot and Corrsin (1971). The vertical line indicates the scale at which the velocity field was filtered to obtain the synthetic large eddy field.

Kolmogorov units in Figure 2. Also shown are the experimental data of Comte-Bellot and Corrsin (1971) at somewhat higher Reynolds number. Agreement with the experimental data between $0.06 < k\eta < 0.4$ indicates that realistic turbulence has been achieved. The tail-up in the simulated spectrum at high wavenumbers indicates some lack of resolution. It is generally believed (Rogallo, 1992) that this will not adversely affect the data in the central portion of the spectrum used here. The vertical line in Figure 2 indicates the scale at which the DNS data was filtered in order to generate the synthetic large eddy field. This scale corresponds to four grid spacings.

For the forced simulation, energy was added to the large scales by including an anti-diffusion term (negative diffusion coefficient) in the Navier-stokes equations. The diffusion coefficient was wavenumber dependent and non-zero only for modes within wavenumber shells less than 3. The value of the coefficient for low wavenumbers was chosen such that the maximum wavenumber, scaled in Kolmogorov units, was unity (i.e. $k_{max}/\eta = 1$). To generate realistic statistically stationary turbulence, the flow was evolved from the random phase initial conditions for approximately 2 large scale eddy turn-over times. The Reynolds number, R_λ, settled at 95.8, while the velocity derivative skewness settled at -0.486. The energy spectrum is shown in Figure 3, where again the vertical line indicates the scale used to generate the large eddy field.

The sgs stresses τ_{ij} and resolved rates of strain $\tilde{S}_{ij}$ and vorticity $\tilde{\omega}_k$ were computed using a spectral cut-off filter with scale r corresponding to 4 grid points. The data
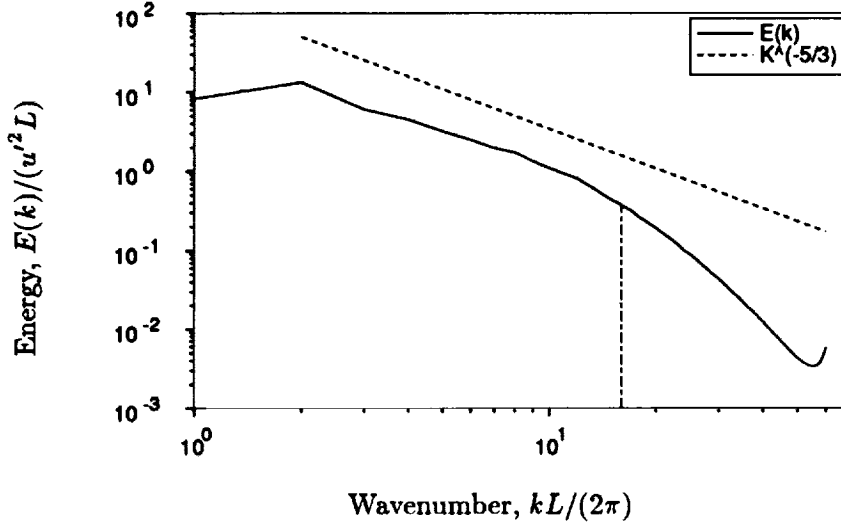
Wavenumber, $kL/(2\pi)$

FIGURE 3.   3-D radial energy spectrum for the forced isotropic turbulence. The vertical line indicates the scale at which the velocity field was filtered to obtain the synthetic large eddy field.

was sampled on every 8th grid point, producing a total of 16^3 realizations. Also computed at each 16^3 point were resolved variables at a scale twice as large as r, $\widehat{S}_{ij}$ and $\widehat{\omega}_k$. The invariants of the tensors were computed as follows:

$$II_{\widetilde{S}} = \sqrt{\widetilde{S}_{mn}\widetilde{S}_{nm}}, \tag{6}$$

$$III_{\widetilde{S}} = (\widetilde{S}_{mn}\widetilde{S}_{np}\widetilde{S}_{pm})^{\frac{1}{3}}, \tag{7}$$

$$II_{\widetilde{R}} = \sqrt{\widetilde{\omega}_k\widetilde{\omega}_k}, \tag{8}$$

and a similar list of invariants for the larger scale rates-of-strain and vorticity.

The search procedure consisted of considering separately each element of the tensor τ as the response variable. Each element of τ, in turn, was assumed to depend on *all* 24 of the predictor variables mentioned above (each element of the tensors plus all invariants). The search is thus a high dimensional one indeed.

It is important to note that when performing independent searches for each element of τ, the resulting model expressions are not expected to be tensorially correct. This weakness stems from the fact that the projection pursuit regression operates most effectively on scalar data. The findings of projection pursuit are still quite valuable, however, since they may be used to guide the construction of tensorially correct models. Such a procedure will be followed here.

3.2 Results

We begin with the decaying field and consider first the normal stress element τ_{11}. To limit the scope of the search, we initially restrict the predictor variables to quantities filtered at scale r. Furthermore, since $\tilde{S}_{ii} = 0$, we eliminate $\tilde{S}_{33}$ from the search, reducing the list to 11 variables.

The main result is the following. The ppreg algorithm finds only one projection (in which the variance of the data around a mean trend is reduced), namely that corresponding to $\tilde{S}_{11}$. The coefficient α corresponding to $\tilde{S}_{11}$ is close to unity, while all others are less than 0.1. The same is true for all other tensor elements, i.e. the only causal dependence appears to be between corresponding elements of τ_{ij} and $\tilde{S}_{ij}$. The smoothed dependence is approximately linear, but the variance about it is still very large. The correlation coefficient between each element of the stress and rate-of-strain tensors is, averaging over all 6 elements, about $\rho = 0.26$. Notice that the Smagorinsky model requires the product between each rate-of-strain element and the second invariant $II_{\tilde{S}}$. Given the discussion in section 2, this could have been detected by the present approach by yielding pairs of projections with similar $|\alpha|$'s for both $II_{\tilde{S}}$ and $\tilde{S}_{ij}$ and canceling parabolic dependences. However, such projections were found to produce more variance than the ones corresponding to constant eddy viscosity. This was checked *a posteriori* by computing the correlation coefficient between each element τ_{ij} and the corresponding term $-II_{\tilde{S}}\tilde{S}_{ij}$. The correlation was marginally smaller than for $\tilde{S}_{ij}$ alone, about $\rho = 0.25$ on average.

The same procedure was repeated for the forced isotropic flow, and the same observations were made. The correlation between τ_{ij} and $\tilde{S}_{ij}$ was even lower (about 0.12 instead of 0.26), but this was again the only causal dependence captured by the algorithm. All other projections did not reduce the variance in any fashion, and correlations with $-II_{\tilde{S}}\tilde{S}_{ij}$ were again smaller than with $\tilde{S}_{ij}$ alone.

Inclusion of the velocity gradients filtered at a larger scale yielded projections that include a weak linear dependence on these gradients but again in terms of the same tensor elements only. In other words, for τ_{11} the 'best' (and only) projection is onto $\tilde{S}_{11} + 0.2\hat{S}_{11}$. Nevertheless, this leaves the correlation virtually unchanged since $\tilde{S}_{11}$ and $\hat{S}_{11}$ are themselves correlated. Similar results were obtained for other tensor elements.

We also considered the possibility that the sgs stresses depend not only on the resolved velocity gradients at the point in question, but at the 26 closest neighboring grid-points as well. To do this, the 6 elements of $\tilde{S}_{ij}$ at each point $\tilde{S}_{ij}(x + i_x r, y + i_y r, z + i_z r)$; $i_x, i_y, i_z = -1, 0, 1$, as well as 3 vorticity components at each of these points was considered. The dimensionality of the space of these predictor variables is 243. It appears unrealistic to expect ppreg to perform adequately in such extreme circumstances. In order to at least explore this direction, we considered $\tau_{11}(x, y, z)$ and investigated how it depends on the first element of the rate-of-strain tensor at all 27 neighboring points on the coarse grid, i.e. the predictor variables were $\tilde{S}_{11}(x + i_x r, y + i_y r, z + i_z r)$, $i_x, i_y, i_z = -1, 0, 1$. The projection pursuit projected again most strongly on $\tilde{S}_{11}(x, y, z)$ ($\alpha = 0.8$), while the α's corresponding to neighboring points were below 0.25. Inclusion of these weak dependencies left the correlation

coefficient virtually unchanged. Since this test is incomplete (one should include all 243 elements in the test) the conclusion that the neighboring velocity gradient does not affect the sgs stresses is somewhat premature. Nevertheless, the partial results obtained here give no indication of any substantial influence.

3.3 The model of Bardina *et al.*

The only model which has been reported to yield high correlations when tested with DNS data is the model of Bardina *et al.* (1983). The correlation between τ_{ij} and $B_{ij} = \widetilde{u_i}\widetilde{u_j} - \widetilde{\widetilde{u}_i}\widetilde{\widetilde{u}_j}$ can be as high as 0.7 to 0.8 when the filter used in creating the synthetic large eddy field from the DNS data is Gaussian. In spite of this, experience shows that when the model is implemented in actual simulations, it dissipates almost no energy, and a Smagorinsky term has to be added (giving the mixed model, Bardina *et al.* 1983). This is puzzling since a high correlation implies at least some alignment between the modeled stress and rate of strain tensor required for dissipation. This issue is addressed below.

Using a Gaussian filter on the decaying isotropic data, we reproduced the quoted correlation of 0.8. We found this result to be misleading, however, since the Gaussian filter produces a 'large-scale' field that contains considerable contributions from the 'small scales', as viewed from a spectral analysis. This 'small scale' information is, of course, not available in an actual large eddy simulation if a spectral method is used. The model of Bardina *et al.* can be viewed as a procedure for extracting the 'small scale' component of the synthetic large eddy velocity field generated from the DNS data. While this procedure yields impressive correlations in tests with DNS data, lack of the 'small scale' component in an actual large eddy simulation field results in a model that may yield a very poor estimate for the real stresses. The near lack of dissipation is probably symptomatic of this.

This hypothesis was tested by experimenting with different filters. We feel that the cut-off filter is the most appropriate for generating the synthetic large eddy field since it completely eliminates the 'small scale' information that will never be present in a spectral large eddy simulation. We have repeated the tests of the model of Bardina *et al.* using a cut-off filter to determine $\widetilde{u}_i$. The second filtering, $\widehat{\widetilde{u}_i}$, was chosen either to be Gaussian or a second cutoff at a scale twice as large as r. Using this scheme, the model of Bardina *et al.* is written as

$$B_{ij}^* = \widetilde{u}_i\widetilde{u}_j - \widehat{\widetilde{u}_i}\,\widehat{\widetilde{u}_j}, \tag{9}$$

As expected, the correlation between the sgs stress and the Bardina model dropped to nearly zero when the cut-off filter was used to generate $\widetilde{u}_i$. This was true independent of the second filter type $(\widehat{\widetilde{u}_i})$. As a consistency check, we found that when B_{ij}^* was included in the projection pursuit as predictor variable, no dependence on this tensor was found.

4. Homogeneous sheared turbulence

In this section, we search for correlations between sgs stresses and resolved variables in homogeneous shear flow. The data was generated by Rogers (1987) on a

128^3 mesh using a variant of the Rogallo code. We considered three different realizations, corresponding to times 10, 12, and 14, in units of the inverse imposed mean shear, $S =< du_1/dx_2 >$. The mean velocity is in the x_1 direction and the mean rotation in the x_3 direction. Cutoff filtering was performed on a scale $r = 4$ grid-points, and every eighth grid point was sampled, as in section 3. The list of predictor variables was again $\tilde{S}_{11}$, $\tilde{S}_{22}$, $\tilde{S}_{12}$, $\tilde{S}_{23}$, $\tilde{S}_{13}$, $\tilde{\omega}_1$, $\tilde{\omega}_2$, $\tilde{\omega}_3$, $II_{\tilde{S}}$, $III_{\tilde{S}}$ and $II_{\tilde{R}} = |\omega|$. Ppreg was repeated 6 times for each element of the sgs stress tensor.

4.1 Results

In contrast to the tests performed in isotropic turbulence, ppreg was able to find several interesting projections in the case of homogeneous shear flow. Table 1 shows the individual tensor elements and the linear combination of predictor variables $z = \alpha_i \ x_i$ that dominate the projections (chosen as those whose $\alpha >$ 0.15). The functional dependence on each projection (f vs z) was found to be fairly linear. The correlation coefficients between τ_{ij} and $-II_{\tilde{S}}\tilde{S}_{ij}$ (Smagorinsky model) are contrasted in the same table with those between τ_{ij} and the dominant elements of the linear combinations found. On average, there is about a 100% improvement above the Smagorinsky model.

Stress	z, (best projection)	$\rho_{[\tau_{ij},-II\tilde{S}_{ij}]}$	$\rho_{[\tau_{ij},z]}$
τ_{11}	$-0.39\tilde{S}_{11}+0.41\tilde{S}_{22}+0.73\tilde{S}_{12}+0.28\tilde{S}_{13}+0.17\tilde{\omega}_2+0.15\tilde{\omega}_3$	0.23	0.36
τ_{22}	$-0.21\tilde{S}_{11}-0.28\tilde{S}_{22}-0.89\tilde{S}_{12}-0.17\tilde{S}_{13}$	0.14	0.23
τ_{33}	$0.76\tilde{S}_{11}-0.2\tilde{S}_{22}+0.24\tilde{S}_{12}-0.23\tilde{S}_{13}-0.157\tilde{\omega}_2-0.44\tilde{\omega}_3$	0.07	0.29
τ_{12}	$-0.66\tilde{S}_{11}-0.2\tilde{S}_{22}-0.7\tilde{S}_{12}$	0.13	0.21
τ_{23}	$0.25\tilde{S}_{11}-0.69\tilde{S}_{23}-0.62\tilde{S}_{13}+0.23\tilde{\omega}_2$	0.06	0.27
τ_{13}	$0.15\tilde{S}_{12}-0.2\tilde{S}_{23}-0.56\tilde{S}_{13}+0.68\tilde{\omega}_1+0.29\tilde{\omega}_2-0.17\tilde{\omega}_3$	0.21	0.34

TABLE 1. Results of projection pursuit for homogeneous shear flow.

It can be appreciated that causal relations exist that are significantly different from the Smagorinsky model. The coefficients showed only minor variations for the other two times considered (St=10 and St=14). This robustness suggests that there is a physical mechanism by which the large-scale field consistently influences the sgs stresses, in addition to what is required energy transfer (i.e. alignment between τ_{ij} and $\tilde{S}_{ij}$). Since the relations tabulated above cannot by themselves provide an adequate relation between tensors, it could be that dependence on other quantities has been omitted. The next section explores the dependence on other quantities that may provide possible mechanisms for the observed degree of causality.

4.2 Dependence on mean shear and modeling

An important consideration when developing a model for the sgs stress is that the resulting model be in the form of a frame invariant tensor. Clearly, the individual terms found in the previous subsection are not invariant under rotations of the coordinate system. A tensorial relation must be found that is consistent with the findings of ppreg on each tensor element. We attempt to find such a tensorial relation in this section. To do this, we first observe that $\tilde{S}_{12}$ and $\tilde{w}_3$ are important contributors in the model for τ_{11}. These tensor elements of $\tilde{S}_{ij}$ and $\tilde{R}_{ij} = -\frac{1}{2}\varepsilon_{ijk}\tilde{\omega}_k$ also correspond to the only non-zero elements in the mean strain-rate and mean rotation tensors. This fact suggests that tensor products of the mean strain rate and mean rotation with the fluctuating strain rate and fluctuating rotation would reproduce some of the dependence found by ppreg for τ_{11}. Analogous reasoning holds for most of the other elements of τ.

To proceed further, we define the mean strain and rotation rate tensors as

$$\Sigma_{ij} = \begin{pmatrix} 0 & \frac{S}{2} & 0 \\ \frac{S}{2} & 0 & 0 \\ 0 & 0 & 0 \end{pmatrix} \tag{10}$$

$$\Omega_{ij} = \begin{pmatrix} 0 & \frac{S}{2} & 0 \\ -\frac{S}{2} & 0 & 0 \\ 0 & 0 & 0 \end{pmatrix} \tag{11}$$

and postulate a model of the following form:

$$\begin{aligned} \tau_{ij}^* = & -2c_1 r^2 II_{\tilde{S}} \tilde{S}_{ij} + \\ & c_2 r^2 (\tilde{S}_{ik}\Sigma_{kj} + \Sigma_{ik}\tilde{S}_{kj})^* + c_3 r^2 (\tilde{R}_{ik}\Omega_{kj} + \Omega_{ik}\tilde{R}_{kj})^* + \\ & c_4 r^2 (\tilde{S}_{ik}\Omega_{kj} - \Omega_{ik}\tilde{S}_{kj}) + c_5 r^2 (\tilde{R}_{ik}\Sigma_{kj} - \Sigma_{ik}\tilde{R}_{kj}), \end{aligned} \tag{12}$$

where $()^*$ indicates trace-free part (note that some of the terms are naturally trace-free). The first (Smagorinsky) term is also present in the ppreg results and thus is included here. To see more clearly how this model reproduces some of the trends of Table 1, note, for instance, that the [11] element of the product between $\tilde{S}_{ij}$ and Σ_{ij} is linear in $\tilde{S}_{12}$ and that between $\tilde{R}_{ij}$ and Ω_{ij} will be linear in ω_3. Again, similar correspondences can be found for other elements of τ.

Since Eq. (12) is linear in the coefficients c_i, these can be determined by the usual least-squares technique. This procedure is easily derived as follows. Write Eq. (12) symbolically as

$$\tau_{ij} = c_k (m_k)_{ij}, \tag{13}$$

where $(m_k)_{ij}$ is the kth trace-free model tensor in Eq (12). When the DNS data is used, the above expression can be compared with the exact trace-free part of the subgrid-scale stress, $(\tau_{ex}^*)_{ij}$. The error in representing the stress via Eq. (13) is given by

$$e_{ij} = (\tau_{ex}^*)_{ij} - c_k(m_k)_{ij}. \tag{14}$$

Assuming the c_k to be constant in space, the global square error is minimized with respect to the c_k by enforcing the following condition

$$\frac{\partial}{\partial c_k} < e_{ij}e_{ij} >= 0, \tag{15}$$

where $<>$ indicates an average over space. This operation leads to the following matrix equation for the c_k

$$c_k = < (m_l)_{ij}(m_k)_{ij} >^{-1} < (m_l)_{ij}(\tau_{ex}^*)_{ij} > \tag{16}$$

Note that this procedure is rather general and does not require that all five terms in Eq (12) be included. Any subset of the five terms can used as a basis and corresponding coefficients solved for via Eq. (16). This feature will be used to determine which combinations of the five terms are most effective in maximizing the correlation between the modeled and exact subgrid-scale stresses.

The quality of the fit is measured in terms of the tensorial correlation coefficient

$$\eta = \frac{< (\tau_{ex}^*)_{ij}M_{ij} >}{\sqrt{< (\tau_{ex}^*)_{ij}(\tau_{ex}^*)_{ij} >< M_{ij}M_{ij} >}}, \tag{17}$$

where $M_{ij} = c_k(m_k)_{ij}$ is the composite model tensor.

The procedure developed above was applied to the homogeneous shear flow data base. Correlation coefficients were determined for all possible combinations of one to five model components. Figure 4 shows the results of this study where the highest correlation coefficient obtained for a given number of model tensors is plotted against the number of tensors used.

The correlation increases as more model tensors are included. The increment in improved correlation, however, deceases as more terms are added. In fact, the correlation coefficient when just three terms are used is nearly identical to that when all five terms are included. This fact suggests that at least two of the terms in Eq. (12) are not particularly useful. The relative importance of the various terms are summarized in Table 2, where the optimal combinations of terms that give rise to the correlations in Figure 4 are listed.

Note that when only one term is used, the optimal choice is not the Smagorinsky model (term 1), but rather term 4, $r^2(\tilde{S}_{ik}\Omega_{kj} - \Omega_{ik}\tilde{S}_{kj})$. For reference, the correlation produced by the Smagorinsky model alone is shown as the square symbol in Figure 4. The Smagorinsky model is seen to be only slightly inferior to term 4. When two or more terms are included, the Smagorinsky model is always present. Terms 2 and 5 enter the list in the last two positions and do not significantly improve the correlation. It is interesting to note that both of these terms contain the mean shear. It is also interesting that terms 3 and 4 are proportional to the mean rotation, and it is these terms that are most effective in increasing the correlation. This point will be discussed further in the following section.
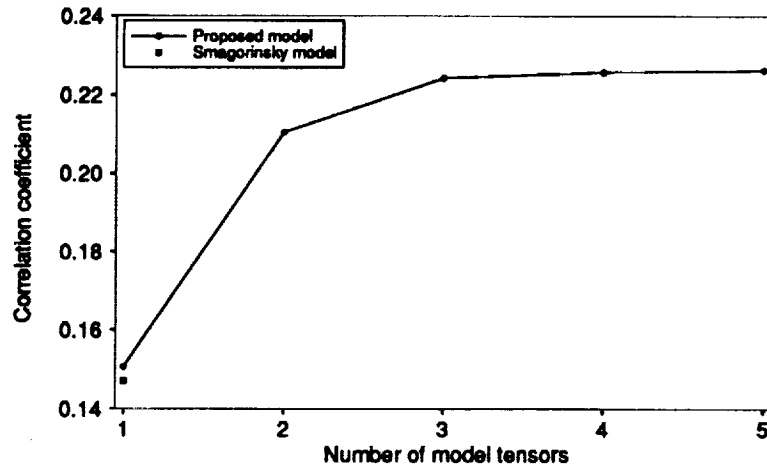
FIGURE 4. Correlation coefficient between the exact homogeneous shear flow sgs stress and subsets of the terms in the model of Eq. (12). For a given number of model tensors, the correlation coefficient plotted is the highest one obtained when all possible combinations of the five terms was considered.

Number of terms	Best combination
1	4
2	1, 4
3	1, 3, 4
4	1, 2, 3, 4
5	1, 2, 3, 4, 5

TABLE 2. Optimal subsets of the model terms in Eq. (12) applied to homogeneous shear flow.

When terms 1, 3, and 4 are used, there is slightly more than a 50% improvement over the Smagorinsky model. This compares with roughly 100% improvement for the tensorially incorrect model listed in Table 1. This discrepancy is due to the fact that not all of the terms contained in Table 1 can be reproduced by the model of Eq. (12). Nevertheless, a simple tensorially correct model was found that captures some of the trends found by projection pursuit.

The coefficients of terms 1, 3, and 4 are 8.52×10^{-3}, -3.03×10^{-2}, and 4.16×10^{-2} respectively.

5. Channel flow

In this section we consider DNS of channel flow. The data were generated with a pseudo-spectral code as detailed in Kim *et al.* (1987). The Reynolds number based on the wall friction velocity was 395, and $256 \times 193 \times 192$ grid points were used. The data was cutoff filtered in the streamwise and spanwise directions only, with a filter size of four grid cells. All results presented here were generated on a single plane of data at $\frac{y}{h} = 0.126$ ($y^+ = 49.8$) where h is the channel half width.

5.1 Results

As a starting point, the correlation between the exact stresses and the Smagorinsky model was investigated. Individual correlation coefficients were computed for each of the tensor elements, and these were found to be very low ($\rho \simeq 0.07$ on average). This trend is shown in Figure 5 in the form of a scatter plot of τ_{12} *vs* $-\tilde{S}_{12}$.
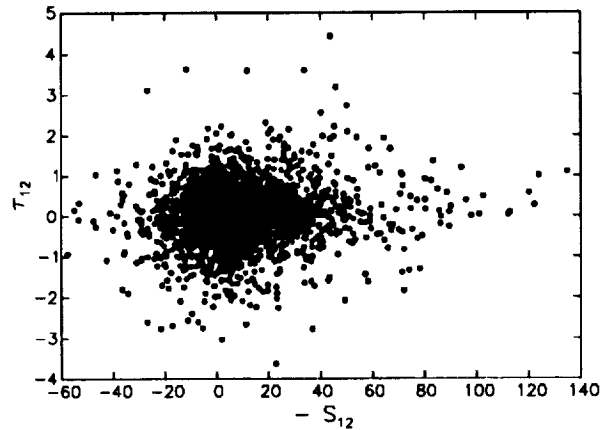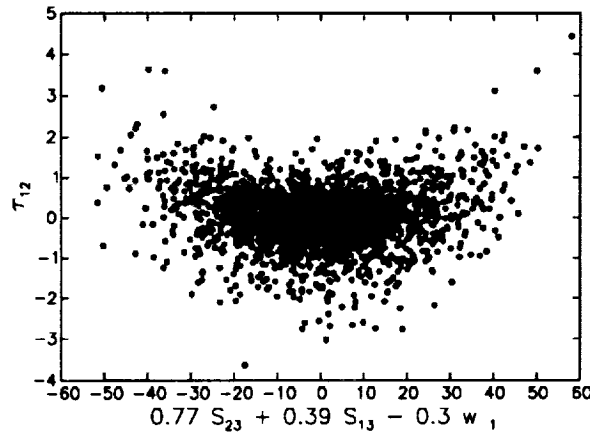

FIGURE 5. Scatter plot of sgs stress τ_{12} as a function of rate-of-strain element $\tilde{S}_{12}$ in DNS of channel flow, at $y/h = 0.126$.

No causal dependence appears to exist between the two variables. The ppreg algorithm was then applied to the data using all elements of $\tilde{S}_{ij}$, $\tilde{\omega}_k$ and the invariants as 11 predictor variables. A sequence of several projections was found for each element of τ_{ij}. This list of projections was reduced to a single one for each element of τ_{ij} by retaining the one that reduced the variance most strongly in each case. These optimal projections are listed in Table 3.

As opposed to the results for homogeneous shear flow, the functional form between τ_{ij} and these projections was found to be non-linear. As an illustration, a scatter plot between τ_{12} and the projection $z_{12} = 0.77\tilde{S}_{23} + 0.39\tilde{S}_{13} - 0.3\tilde{\omega}_1$ is shown in Figure 6. The main trend of τ_{12} as a function of z_{12} appears to be quadratic.

Stress	z, (best projection)	$\rho_{[\tau_{ij}, -II\tilde{S}_{ij}]}$	$\rho_{[\tau_{ij}, z^2]}$
τ_{11}	$-0.8\tilde{S}_{13} + 0.51\tilde{\omega}_2$	0.12	0.44
τ_{22}	$-0.4\tilde{S}_{22} - 0.86II_{\tilde{S}}$	0.10	0.21
τ_{33}	$0.45\tilde{S}_{23} + 0.85\tilde{S}_{13} + 0.17\tilde{\omega}_2$	0.02	0.36
τ_{12}	$0.77\tilde{S}_{23} + 0.39\tilde{S}_{13} - 0.3\tilde{\omega}_1$	0.10	0.34
τ_{23}	$-0.51\tilde{S}_{11} - 0.43\tilde{S}_{22} + 0.35\tilde{S}_{12} +$ $0.47\tilde{S}_{23} - 0.29\tilde{S}_{13} - 0.17(\tilde{\omega}_1 - \tilde{\omega}_2 + \tilde{\omega}_3)$	0.05	0.27
τ_{13}	$0.82\tilde{S}_{11} + 0.48\tilde{S}_{22} - 0.23\tilde{\omega}_2$	0.05	0.31

TABLE 3. Results of projection pursuit for channel flow.

FIGURE 6.   Scatter plot of sgs stress τ_{12} as a function of best projection onto elements of filtered velocity gradient tensor, found by ppreg.   Same data as in Figure 5.

Similar behavior was found for all other tensor elements, the trend being strongest for the [11], [33], [12], and [13] components. To quantify the causality between the stresses and the corresponding z's, the correlation coefficients between individual elements of τ and the corresponding z^2 were computed. Since each of the observed quadratic trends had a minimum close to the origin, it is sufficient to consider the single term z^2. These correlation coefficients appear in the last column of Table 3. Notice that when compared with the correlation produced by the Smagorinsky model, more than a four-fold increase is detected. This trend can also be observed

by comparing Figure 5 to Figure 6.

5.2 Modeling

As in section 4.2, the expressions in Table 3 are by themselves not valid relations between tensors. Unlike the linear relationship found in shear flow, the elements of τ depend quadratically on the projections in channel flow. For example, the model for τ_{12} is $(0.77\tilde{S}_{23} + 0.39\tilde{S}_{13} - 0.3\tilde{\omega}_1)^2$. The tensor model found for homogeneous shear flow may not be of much use in this case since it is not able to produce the non-linear products that result from squaring the projection. The quadratic non-linearities suggest that it may be possible to model the stresses in terms of various tensor products of the strain and rotation rates. Such a model is

$$
\begin{aligned}
\tau_{ij}^* = & -2c_1 r^2 II_{\tilde{S}}\tilde{S}_{ij} + \\
& c_2 r^2 (\tilde{S}_{ik}\tilde{S}_{kj})^* + c_3 r^2 (\tilde{R}_{ik}\tilde{R}_{kj})^* + \\
& c_4 r^2 (\tilde{S}_{ik}\tilde{R}_{kj} - \tilde{R}_{ik}\tilde{S}_{kj}) + c_5 r^2 (\tilde{S}_{ik}\tilde{S}_{kl}\tilde{R}_{lj} - \tilde{R}_{ik}\tilde{S}_{kl}\tilde{S}_{lj})/II_{\tilde{S}},
\end{aligned}
\tag{18}
$$

where $()^*$ again indicates trace-free part. This model was studied by Lund and Novikov (1992) and represents the most general relation between the subgrid-scale stress and the strain and rotation rate tensors.

The least-squares fitting procedure was applied to the above model as well as the model of Eq. (12). The resulting correlation coefficients are shown in Figure 7.
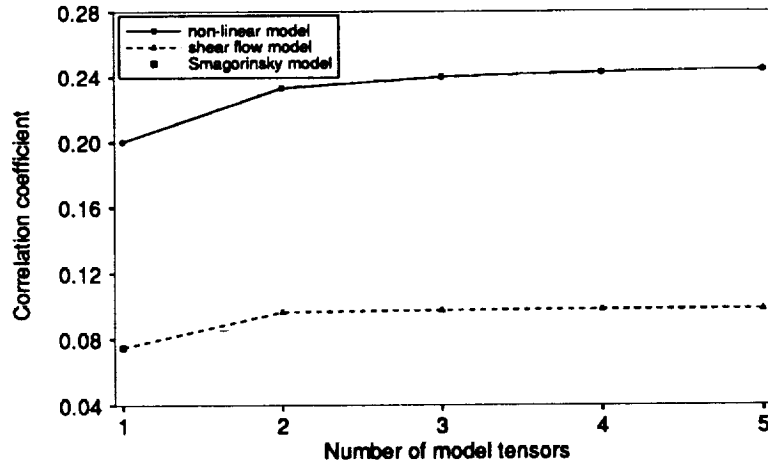

FIGURE 7. Correlation coefficients for the terms in the models of Eqs (12) and (18) applied to channel flow data.

As expected, the model developed for shear flow (Eq. (12)) does not offer much improvement here. The non-linear model of Eq (18), on the other hand, considerably

Number of terms	Best combination
1	4
2	3, 4
3	1, 3, 4
4	1, 3, 4, 5
5	1, 2, 3, 4, 5

TABLE 4. Optimal subsets of the model terms in Eq. (18) applied to channel flow.

increases the correlation relative to the Smagorinsky model. As in the shear flow case, only two or three terms contribute significantly to the increase in correlation coefficient. The ranking of terms in Eq. (18) is summarized in Table 4.

As in the shear flow, the Smagorinsky model does not produce the highest correlation when used in isolation. In fact, it produces the lowest correlation of any single term, while term 4, the best one, produces a correlation coefficient that is roughly 2.7 times higher! Furthermore, the Smagorinsky model does not enter the list until three or more terms are included and adds little to the correlation at that point. When three terms are included, the correlation coefficient is about 3.2 times higher than that provided by the Smagorinsky model. This compares with an average of improvement of a factor of 4.4 obtained by the projection pursuit algorithm. Thus the model of Eq. (18) incorporates quite well the findings of projection pursuit into a tensorially correct model.

As in the shear flow, the rotation rate enters as an important parameter. In both the shear and channel flow, the best single term is the product of strain and rotation rate (actually, it is the mean rotation in the shear flow and the local rotation in the channel flow). The observed strong dependence on this term is perhaps not too surprising since it is representative of vortex stretching. Although there is a connection with vortex stretching, the strain, rotation product does not remove energy from the large scales (*i.e.* $(\tilde{S}_{ik}\tilde{R}_{k,j} - \tilde{R}_{ik}\tilde{S}_{kj})\tilde{S}_{ij} = 0$). Thus, by itself, this term would not be a useful model, and a term that has a non-zero projection on the strain rate (such as the Smagorinsky model) must be added.

The coefficients of terms 1, 3, and 4 are 1.13×10^{-3}, -1.38×10^{-2}, and -8.71×10^{-3} respectively.

The above collection of predictor variables is by no means exhaustive. Examples of other dependencies that could have been included are the mean velocity gradients Σ_{ij} and Ω_{ij} and the distance from the wall λ_i (a vector).

6. Summary and conclusions

A novel regression algorithm has been used to explore DNS data in an effort to determine improved models that parameterize the sgs stresses for large eddy

simulation. In addition to the rate of strain, several other variables have been considered. These include rotation, velocity gradients filtered at larger scales, and velocity gradients at neighboring points as well as the invariants of the strain and rotation rate tensors. DNS data from isotropic turbulence, homogeneous shear flow, and turbulent channel flow have been considered.

For isotropic turbulence, no statistically robust relations were found other than the small correlation between the stress and rate-of-strain tensor required for energy transfer. This finding may imply that, other than the weak relation between the stress and rate of strain, the large-scale velocity gradients in isotropic flow do not dictate the behavior of the small scales giving rise to the sgs stresses. Given that the ppreg algorithm is not guaranteed to find *all* existing trends, we can not state this conclusion with absolute certainty. Nevertheless, it is very likely that for the Reynolds number range considered, there is no strong, simple connection between large scale velocity gradients and sgs stresses in isotropic turbulence.

Entirely different behavior was observed in turbulent shear flows. Individual components of the stress tensor were found to depend on several elements of the fluctuating strain and rotation rate tensors. The dependence was found to be linear in the case of homogeneous shear flow and quadratic in the case of channel flow. In the case of homogeneous shear flow, the observed dependence was used to guide the construction of a model that involved tensor products of the mean strain and rotation rate with their fluctuating counterparts. This model was shown to produce a correlation between modeled and exact stresses that was 50% higher than that given by the Smagorinsky model. The proposed model for homogeneous shear flow did not carry over to channel flow, and only marginal improvement over the Smagorinsky model was observed. The results of projection pursuit were again used to guide the construction of a model for channel flow. This model was considerably more successful, yielding more than a 200% improvement over the Smagorinsky model. Whereas the shear flow model did not extend well to channel flow, the channel flow model did perform reasonably well in shear flow, yielding correlations that were roughly 90% of those achieved with the shear flow model.

One interesting finding of this work is that mean strain and rotation rates enter in the parameterization of the subgrid-scale stresses, at least in the case of homogeneous shear flow. This is at variance with the view that at large Reynolds numbers the small scales should be nearly isotropic and unaligned with the large-scale motions (Kolmogorov, 1941). Indeed, recent experimental measurements of Saddoughi (1992) confirm small-scale isotropy at high *Re*. Of course, the low Reynolds number data used here does not provide a sufficient range of scales to realize small scale isotropy, and, consequently, the subgrid scales have some residual alignment with the mean gradients. It is thus conceivable that the observed dependence on the mean quantities would disappear if the Reynolds number and hence the scale separation were increased.

On the other hand, it is not clear that traditional measures of isotropy (spectra, structure functions etc.) have a direct connection with the behavior of the sgs stresses. Alternately, the observed dependence on the mean quantities could also

be present in a slightly different form at higher Reynolds number. In this view, the shear and rotation produced by large scales of size, say, br (where r is the filter size and $b > 2$) may take on the role of mean shear and rotation as far as the small scales are concerned. We did not find such trends in the isotropic flow using $b = 2$, but it is possible that such a trend requires large separation ($b >> 2$) and higher Re. Unfortunately, this issue cannot be addressed using DNS data at low Reynolds numbers.

Acknowledgements

REFERENCES

BARDINA G.   1983 Improved turbulence models based on large eddy simulation of homogeneous, incompressible, turbulent flows, Ph.D. thesis, report TF-19, Mechanical Engineering, Stanford Univ.

CLARK R. A., FERZIGER J. H., & REYNOLDS W. C.   1979 Evaluation of subgrid-scale models using an accurately simulated turbulent flow. *J. Fluid Mech.* **91**, 1.

COMTE-BELLOT, G., & CORRSIN, S.   1971 Simple Eulerian time correlation of full and narrow-band velocity signals in grid-generated 'isotropic' turbulence. *J Fluid Mech.* **48**, 273-337.

FRIEDMAN J.H. & STUETZLE W.   1981 Projection pursuit regression. *J. Amer. Stat. Assoc.* **76**, 817.

GERMANO M., PIOMELLI, U., CABOT, W., AND MOIN, P.,   1991 A dynamic subgrid-scale eddy viscosity model. *Phys. Fluids A.* **3**, 1760-1765.

KIM, J., MOIN, P., AND MOSER, R. D.,   1987 Turbulence statistics in fully developed channel flow at low Reynolds number. *J. Fluid Mech.* **177**, 133.

KOLMOGOROV A. N. 1941 Local structure of turbulence in an incompressible fluid at very high Reynolds number. *Dokl. AN SSSR.* **30**, 299.

LUND T. & NOVIKOV E.A.   1992 Parameterization of subgrid-scale stresses by the velocity gradient tensor, in preparation.

McMILLAN O.J. & FERZIGER J.H 1979 Direct testing of subgrid-scale models. *AIAA J.* **17**, 1340.

PIOMELLI U., MOIN P. & FERZIGER J.H. 1988 Model consistency in large eddy simulation of turbulent channel flows. *Phys. Fluids.* **31**, 1884.

ROGALLO R. 1981 Numerical experiments in homogeneous turbulence. *NASA Tech. Mem. 81315.*

ROGERS, M. M. & MOIN, P. 1987 The structure of the vorticity field in homogeneous turbulent flows. *J Fluid Mech.* **176**, 33-66.

ROGALLO R. 1992 private communication.

SADDOUGHI, S. G., 1992 Experimental investigation of local isotropy in high Reynolds number turbulence. *CTR Annual Research Briefs*, Stanford Univ./ NASA Ames.